Astroparticle Physics 42 (2013) 33–40

Contents lists available at SciVerse ScienceDirect

Astroparticle Physics

journal homepage: www.elsevier.com/locate/astropart

A study of the performance parameters of the High Altitude Gamma Ray (HAGAR) telescope system at Ladakh in India

L. Saha [a,*], V.R. Chitnis [b], P.R. Vishwanath [c], S. Kale [c], A. Shukla [c], B.S. Acharya [b], G.C. Anupama [c], P. Bhattacharjee [a], R.J. Britto [a,b], T.P. Prabhu [c], B.B. Singh [b]

[a] Saha Institute of Nuclear Physics, 1/AF, Bidhannagar, Kolkata 700 064, India
[b] Tata Institute of Fundamental Research, Homi Bhabha Road, Colaba, Mumbai 400 005, India
[c] Indian Institute of Astrophysics, II Block, Koramangala, Bangalore 560 034, India

ARTICLE INFO

Article history:
Received 12 July 2012
Received in revised form 10 October 2012
Accepted 19 November 2012
Available online 5 December 2012

Keywords:
Atmospheric Cherenkov technique
Extensive air shower simulations
γ-Ray astronomy

ABSTRACT

We present results of Monte Carlo simulations for the High Altitude Gamma Ray (HAGAR) telescope array which detects very high energy gamma rays from astronomical sources. This telescope array, located at Hanle at an altitude of 4270 m in the Ladakh region of the Himalayas in India, is the highest altitude atmospheric Cherenkov experiment in the world. Taking advantage of the high altitude, this experiment could achieve relatively low energy threshold with a modest mirror area coverage. To understand the performance parameters of this telescope system, we have simulated large samples of extensive air showers initiated by gamma rays and various species of cosmic rays, using the CORSIKA package. Cherenkov photons produced in the atmosphere are sampled at ground level. These photons are then passed through the detector simulation program, which takes into account various design details and the data acquisition system of HAGAR. Night sky photons are also considered in the detector simulation program as performance of the telescope depends strongly on the level of night sky background (NSB) at the observation site. We have estimated various performance parameters like energy threshold and effective area for vertically incident showers as well as inclined showers. Details of these parameters, results obtained from simulations and comparison with the observed data are presented. It is shown that the energy threshold of the HAGAR telescope system is about 208 GeV, a factor of $\sim$4 less than for a similar set up at about 1000 m altitude, and it is able to detect Crab like sources at 5σ significance in 17 h of observation without imposing additional criteria, like gamma-hadron separation, for further rejection of cosmic rays.

1. Introduction

High Altitude GAmma Ray (HAGAR) telescope system is designed to detect very high energy gamma rays from astronomical sources through atmospheric Cherenkov technique. This technique of counting atmospheric Cherenkov photons using single PMT and mirror was pioneered by Galbraith and Jelly in 1953 [1]. HAGAR is based on nonimaging atmospheric Cherenkov technique which measures arrival time of Cherenkov shower front at various locations in the Cherenkov light pool using an array of telescopes. From the arrival time information, direction of shower axis is estimated to enable rejection of off-axis cosmic ray showers. HAGAR telescope system consists of an array of seven telescopes located at Hanle (32°46′46″ N, 78°58′35″ E, 4270 m above msl), Ladakh, in the Himalayas. HAGAR is the highest altitude atmospheric Cherenkov telescope in the world. Taking advantage of the high altitude, this experiment achieves a comparatively low energy threshold of 208 GeV with a modest mirror area of 31 m^2. Regular source observations have been going on with the complete set up of seven telescopes since September 2008. Estimation of the sensitivity of the experiment is in an advanced stage, using data taken for a prolonged period from the Crab nebula, the standard candle source of TeV gamma rays. In this article we present details of Monte Carlo simulations done to obtain the performance parameters of the HAGAR telescope system. We also compare the simulation results with the results obtained from experimental data.

The rest of the paper is organized as follows: in Section 2 we describe the details of HAGAR telescope array. The simulations of atmospheric air showers and detector response are discussed in Section 3. Performance of the detector and comparison of simulation results with data are discussed in Sections 4 and 5 respectively. We end with a summary and conclusion in Section 6.

* Corresponding author.
E-mail address: lab.saha@saha.ac.in (L. Saha).

0927-6505/$ - see front matter © 2012 Elsevier B.V. All rights reserved.
http://dx.doi.org/10.1016/j.astropartphys.2012.11.012

2. Details of HAGAR telescope array

The HAGAR array [2] consists of seven telescopes of which six are deployed at the vertices of a hexagon, with the seventh one placed at the center of the hexagon (see Fig. 1). Each telescope consists of seven front coated parabolic mirrors each of diameter 0.9 m. The mirrors are of parabolic shape with f/d ratio of 1 and are fabricated from 10 mm thick float glass sheets. All the seven mirrors of each telescope are mounted para-axially on a single platform while the telescopes themselves are mounted alt-azimuthally. A photo multiplier tube (PMT) of type XP2268B manufactured by Photonis is kept at the focus of each mirror. The diameter of PMT photo cathode defines the field of view to be 3° at FWHM. This PMT has good sensitivity to photons in the ultraviolet to blue range, with peak quantum efficiency of about 24% at 400 nm. Pulses from the photo-tubes are brought to control room situated below the central telescope via coaxial cables of length 85 m and of types LMR-ultraflex-400 (of length 30 m) and RG 213 (of length 55 m).

Each of the telescope axes is driven by a stepper motor. The telescope movement control system consists of two 17-bit Rotary encoders, two stepper motors and a micro-controller based Motion Control Interface Unit (MCIU). Steady state pointing accuracy of the servo is ±10 arc-sec with maximum slew rate of 30°/min. The resulting blind spot size while tracking the stars near zenith is found to be less than 0.6°. The telescope movement is maneuvered by a control software written on Linux platform. The pointing of the telescope is continuously monitored and corrected in real time during tracking [3].

High voltages fed to photo tubes are controlled and monitored using C.A.E.N controller (model SY1527). PMT pulses are given to CAMAC based interrupt driven system in control room which acquires and records the data. During observations, count rates from individual PMTs are adjusted to 5000 counts/s for discriminator bias of 150 mV. Equality of PMT rates ensures equal efficiency for each channel. For trigger formation, analog addition of pulses from seven PMTs of each telescope is performed within accuracy of 1 ns to get seven telescope pulses also called Royal Sum (RS) pulses. Event trigger is generated if there is a coincidence of at least 4 RS pulses out of 7, above a pre-assigned threshold, within a time window of 150 ns to 300 ns depending on the zenith angle of the pointing direction. RS discriminator biases are adjusted to keep the RS rates within 25–35 kHz to maintain a chance coincidence rate within a few percent of the trigger rate. Data recorded on event interrupt includes relative arrival time of a shower front recorded by the TDCs accurate to 0.25 ns. Cherenkov photon density at each telescope, given by the total charge in PMT pulses, is recorded using 12 bit QDCs. An absolute arrival time of an event accurate to μs is given by a Real Time Clock (RTC) module synchronized with GPS. Various other information, such as the triggered telescopes in an event, are also recorded. In addition to this, the rates from 49 PMTs as well as RS rates are monitored continually and recorded at regular intervals using monitoring interrupts of frequency 1 Hz.

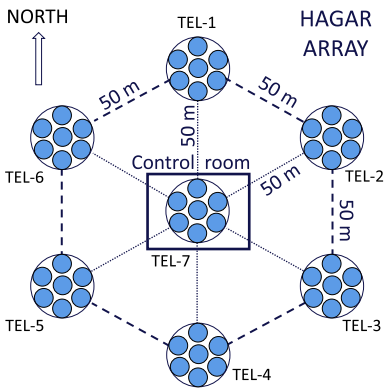

Fig. 1. A schematic diagram of HAGAR telescope array setup.

3. Monte Carlo simulations

Simulation plays a very important role in this kind of very high energy γ-ray experiments. Since very high energy gamma rays cannot be produced in laboratory, direct calibration is not possible for the instruments. So, we have to understand the performance of the instruments only by estimating various performance parameters from simulations. We used the publicly available software package CORSIKA to simulate air showers. The detector simulation software has been developed in house. A preliminary discussion about simulations and performance parameters of the HAGAR telescope system was given in [4,5]; the details of the simulation are described here.

3.1. Atmospheric air shower simulations

CORSIKA [6,7] is a Monte Carlo program for studying the evolution of extensive air shower (EAS) in the atmosphere initiated by photons and various species of charged particles including protons, alpha particles and other nuclei. We use CORSIKA version 6.720 for atmospheric air shower simulations. VENUS [8] code is used for high energy hadronic interactions and GHEISHA [9] program is used for the low energy hadronic interactions. For electromagnetic interactions EGS4 [10] program is used. We used our detector geometry in input data card choosing IACT [11] option in CORSIKA. We do not have measurements of atmospheric profile at the Hanle site yet. So we have used the US standard atmospheric profile as best possible choice for generation of Cherenkov photons. Wavelength dependent absorptions of Cherenkov photons caused by atmosphere, reflectivity of mirrors (average value of 80%) and quantum efficiency of PMT are given as input in CORSIKA. Information about Cherenkov photons with wavelength in the range of 200–650 nm is stored. Impact parameter is varied over the range of 0–300 m and viewcone is kept at 0° around the pointing direction for gamma ray initiated showers and varied over 0°–4° for cosmic ray generated showers. Azimuthal angle is selected over the range of 0° –360°. Showers initiated by gamma rays, protons, alpha particles and electrons are simulated using following primary spectral shapes ([12,13]):

$$\frac{dN_\gamma}{dE} = 3.27 \times 10^{-7} E^{-2.49}\ \mathrm{TeV}^{-1}\ \mathrm{m}^{-2}\ \mathrm{s}^{-1},$$

$$\frac{dN_p}{dE} = 8.73 \times 10^{-2} E^{-2.7}\ \mathrm{TeV}^{-1}\ \mathrm{m}^{-2}\ \mathrm{s}^{-1}\ \mathrm{sr}^{-1},$$

$$\frac{dN_\alpha}{dE} = 5.71 \times 10^{-2} E^{-2.6}\ \mathrm{m}^{-1}\ \mathrm{m}^{-2}\ \mathrm{s}^{-1}\ \mathrm{sr}^{-1},$$

$$\frac{dN_e}{dE} = 11.5 \times 10^{-5} E^{-3.08}\ \mathrm{TeV}^{-1}\ \mathrm{m}^{-2}\ \mathrm{s}^{-1}\ \mathrm{sr}^{-1},$$

respectively. The spectral index of the primary γ-rays (2.49) is used in accordance with the energy spectrum of Crab nebula derived from Whipple data [14]. Spectral shape measured by Whipple is consistent with measurements from HEGRA [15] and MAGIC above 200 GeV [16]. Energies of primary particles are selected using random numbers distributed according to the power law energy spectrum given above. Geomagnetic field used is appropriate for the Hanle location with the horizontal and vertical components of the

Table 1
Samples generated for vertical showers.

Type	Energy range GeV	# of showers generated
Gamma rays	20–5000	1×10^6
Protons	50–5000	3×10^6
Alpha particles	100–10000	6×10^6
Electrons	20–5000	3×10^5

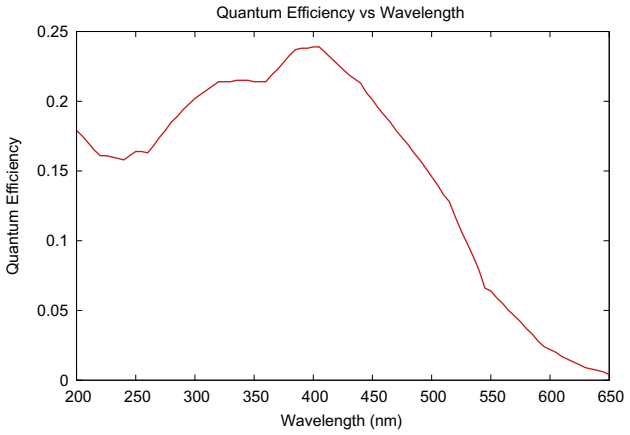

Fig. 2. Quantum efficiency plot for PMT (XP2268B).

magnetic field being $B_x = 32.94$ μT and $B_z = 38.58$ μT, respectively. Altitude of Hanle is taken to be 4270 m. HAGAR telescope array geometry as described in previous section is used.

The number of showers generated using above input parameters and energy ranges used in simulations are given in Table 1 for vertically incident showers. We have also simulated showers for inclination angles of 10°, 15°, 20°, 30°, 40°, and 45°. The simulations give the positions of Cherenkov photons at the ground level along with their direction cosines. For vertical showers the telescopes are pointed towards the zenith. So the X–Y coordinates of photons on the mirror plane are same as those at ground level. But for inclined showers we have calculated arrival times and locations of Cherenkov photons in the telescope plane using appropriate transformations. The details of this coordinate transformation procedure for this kind of telescopes can be found in [17]. Finally, the CORSIKA simulations give the information about the number of Cherenkov photons falling on the mirrors, their arrival angle and arrival time.

3.2. Detector simulation

CORSIKA simulation gives information about arrival time of Cherenkov photons at each PMT. This information is then passed through the detector simulation program. This program takes into account details of the HAGAR system including PMTs, coaxial cables, trigger formation etc. In addition to Cherenkov photons, we must also take into account the night sky background (NSB) photons. The NSB photons are simulated assuming a flux of 2×10^8 ph cm^{-2} s^{-1} sr^{-1} in the wavelength range of 200–650 nm, measured at Hanle using single photo-electron counting technique.[1] NSB photons are simulated in 0.2 ns bins using Poissonian distribution around this measured value and following typical wavelength dependence of NSB given in [18] . For this purpose we have used a functional fit to the data given in [18] to obtain the NSB distribution function, which has the following form:

$$f(\lambda) = -161.92695 + 0.237421\lambda - 0.0001422\lambda^2 + 4.46152 \times 10^{-08}\lambda^3 - 7.72914 \times 10^{-12}\lambda^4 + 7.01583 \times 10^{-16}\lambda^5 - 2.60706 \times 10^{-20}\lambda^6. \quad (1)$$

Here λ is wavelength of the photons in units of Angstrom. The NSB photons are added to Cherenkov photons which are obtained from CORSIKA simulations. CORSIKA allows conversion of the Cherenkov photons into photoelectrons according to quantum efficiency curve for the PMT (see Fig. 2). Similarly each NSB photon is converted into photoelectron using the same quantum efficiency curve according to the wavelength assigned to the photon using Eq. (1). PMT response function for single photo electron measured in laboratory is approximated with a Gaussian with rise time of 3.0 ns and FWHM of 4.2 ns as given by

$$f(t) = \frac{1}{\sigma\sqrt{2\pi}} \exp\frac{-(t-t_0)^2}{2\sigma^2}, \quad (2)$$

where t_0= 6.7 ns . The PMT integration time is taken to be 10.5 ns.

The PMT pulses are generated by convolving the number of photoelectrons in each bin with the above PMT response function. The pulse shape profile is converted to voltage $v(t)$ using the relation, $v(t) = iRf(t)$, where, i is PMT current, R is load resistance of PMT and $f(t)$ is the pulse profile due to the single photo electron (Eq. 2). The PMT load resistance is kept at 50 ohms, and the PMT current, i, is calculated using the relation, $i = g/(e \times \mathrm{FWHM})$, where e is the electron charge and g is the PMT gain. We use an average PMT gain of 6.78×10^5. Attenuation of these pulses in coaxial cables (30 m of LMR-Ultraflex-400 and 55 m of RG213) is taken into consideration using frequency dependence of attenuation provided by manufacturer. Trigger is generated when at least 4 RS pulses out of 7 cross the discriminator threshold of 220 mV in a coincidence window of 150 ns for showers within zenith angles of 30°. For lager zenith angles coincidence window of 300 ns is used. In terms of photo-electrons this discriminator threshold corresponds to 17.5 photo-electrons per telescope. Once a trigger is generated, TDC and QDC values are calculated using various calibrations carried out with the HAGAR setup. These values are written to output file.

4. Performance parameters

4.1. Trigger rate

HAGAR trigger is generated when at least 4 telescope pulses out of 7 cross a discriminator threshold within a narrow coincidence window. Performance parameters are estimated for this condition ($\geqslant$4) as well as for other trigger conditions involving at least 5 telescopes ($\geqslant$5), at least 6 telescopes ($\geqslant$6) and all 7 telescopes (=7) triggering. Performance parameters for various trigger conditions for vertically incident showers are given in Table 2 and those for various zenith angles are given in Table 3 (for $\geqslant$4 trigger condition only).

Table 2
Performance parameter for HAGAR telescope array for vertical shower.

Trigger condition	Proton trigger rate (Hz)	Alpha trigger rate (Hz)	Electron trigger rate (Hz)	Gamma ray rate (/min)	γ-Ray energy threshold (GeV)	Effective area for γ-rays (m^2)	Observed trigger rate (Hz)
$\geqslant$ 4	9.2	3.7	0.11	6.3	208	3.2×10^4	13.4 ± 0.2
$\geqslant$ 5	4.5	2.7	0.05	3.9	234	2.4×10^4	8.5 ± 0.1
$\geqslant$ 6	2.2	1.6	0.03	2.4	263	1.7×10^4	4.9 ± 0.1
=7	1.1	0.9	0.01	1.5	275	1.2×10^4	2.4 ± 0.1

[1] NSB flux measured at Hanle varied between (0.8 and 2) $\times 10^8$ ph cm^{-2} s^{-1} sr^{-1} depending on the region of the sky as well as on the season.

Table 3
Performance parameters for various zenith angles for the $\geqslant 4$ trigger condition.

Zenith angle (°)	Proton trigger rate (Hz)	Alpha trigger rate (Hz)	Gamma ray rate (/min)	γ-Ray energy threshold (GeV)	Effective area for γ-rays (m^2)	Observed trigger rate (Hz)
0	9.2	3.7	6.3	208	3.2×10^4	13.4 ± 0.2
15	9.1	3.7	6.4	234	3.4×10^4	12.9 ± 0.5
30	8.9	2.9	5.0	316	4.4×10^4	11.7 ± 1.0
45	6.8	2.7	3.8	549	7.8×10^4	10.1 ± 1.6

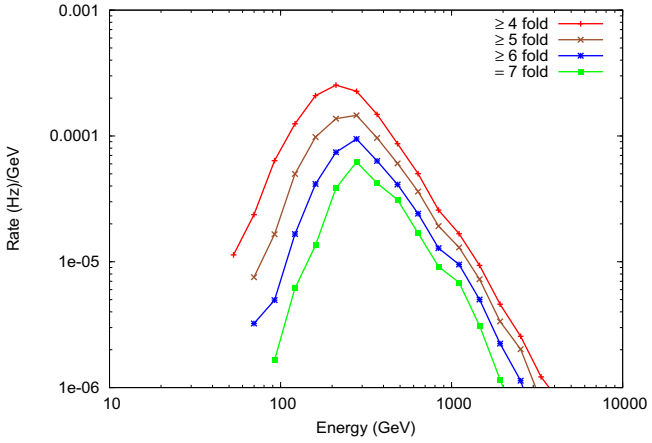

Fig. 3. Differential rate plot for different trigger conditions.

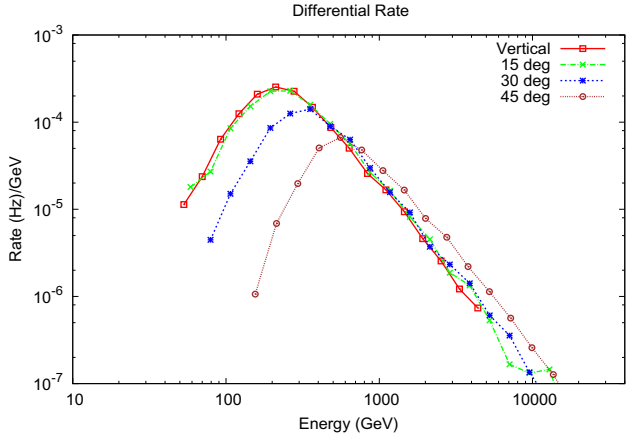

Fig. 4. Differential rate plot for different zenith angle for the $\geqslant 4$ trigger condition.

Cosmic ray trigger rate estimated from simulations, assuming that bulk of the triggers come from protons, alpha particles and electrons, is 13 Hz for $\geqslant 4$ trigger condition. This matches very well with the observed trigger rate from HAGAR for near vertical showers. Expected gamma ray rate for Crab like source at near vertical position is 6.3 counts/min. Trigger rate decreases for higher fold trigger conditions as seen from Table 2. It also decreases for higher zenith angles as seen from Table 3.

4.2. Energy threshold

The Energy threshold of HAGAR is obtained from the differential rate plot (Fig. 3 and Fig. 4). The energy corresponding to peak of the differential rate curve is conventionally quoted as energy threshold. Differential rate curves for various trigger conditions and for different zenith angles are shown in Fig. 3 and Fig. 4 respectively. Values of the energy threshold so obtained for various conditions and zenith angles are listed in Tables 2 and 3. In the case of vertically incident gamma rays, energy threshold is about 208 GeV for

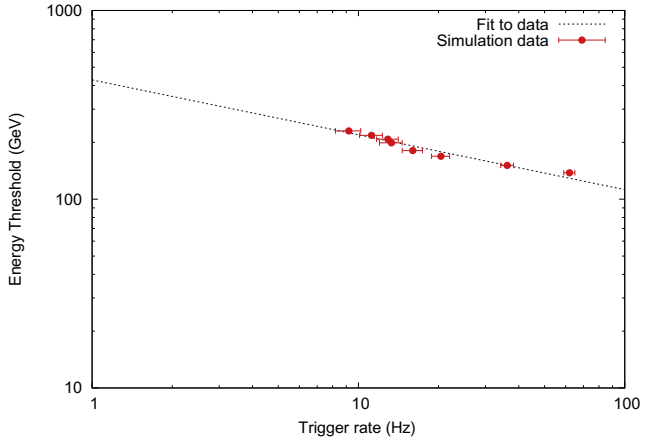

Fig. 5. Energy threshold vs trigger rate from MC.

Table 4
Variation of trigger rate and energy threshold with discriminator bias.

Discriminator threshold (mV)	Photo-electron threshold	Trigger rate (Hz)	γ-Ray energy threshold (GeV)
170	13.5	62.0	138
180	14.3	36.2	151
190	15.1	20.4	169
200	15.8	16.0	181
210	16.7	13.3	199
220	17.5	13.0	208
230	18.3	11.2	218
240	19.0	9.2	230

Table 5
Variation of trigger rate and energy threshold with NSB flux level.

NSB($\times 10^8 cm^{-2} s^{-1} sr^{-1}$)	Trigger rate (Hz)	γ-Ray energy threshold (GeV)
1.0	20.7	158
1.5	15.8	177
2.0	13.0	208
2.5	9.3	251

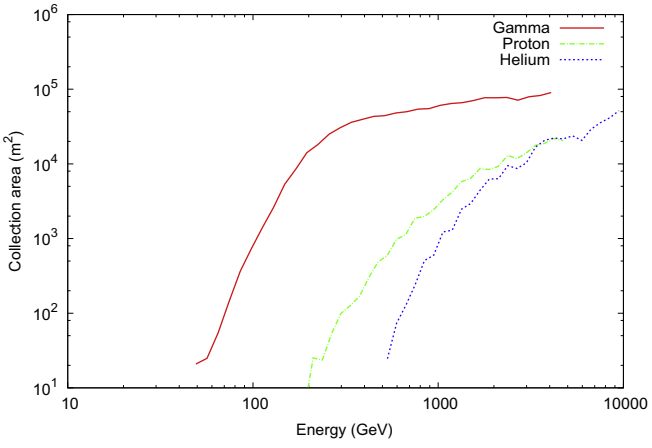

Fig. 6. Effective area vs energy of primary from MC for vertical incidence.

Table 6
Dependence of the threshold energy and collection area on the spectral shapes of γ-ray energy spectrum.

Spectral index	γ-Ray energy threshold (GeV)	Effective area for γ-rays (m^2)
2.0	223	3.6×10^4
2.2	223	3.5×10^4
2.4	213	3.3×10^4
2.49	208	3.2×10^4
2.6	199	3.0×10^4
2.8	190	2.7×10^4
3.0	173	2.3×10^4

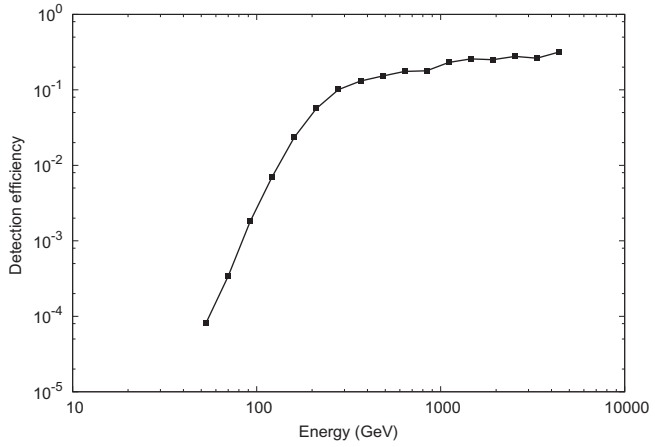

Fig. 7. Detection efficiency vs energy for γ-rays from simulations for $\geqslant$4-fold trigger condition.

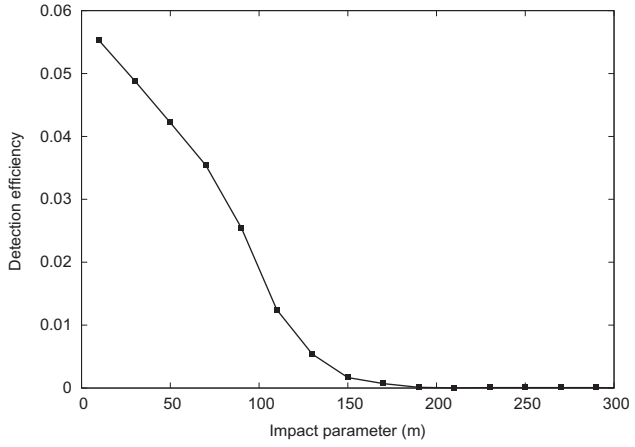

Fig. 8. Detection efficiency vs impact parameter for γ-rays from simulations for $\geqslant$4-fold trigger condition.

$\geqslant$4 trigger condition and increases at higher trigger condition. This is because, in order to trigger larger number of telescopes, the Cherenkov photon density must be higher, which requires higher energy showers. Also, as we go to higher zenith angle, the showers need to travel through larger atmospheric mass. Hence, atmospheric attenuation becomes more effective for higher zenith angle. As a result, higher energy showers are required to trigger the system. Threshold for $\geqslant$4 trigger condition increases from 208 GeV near vertical to 549 GeV for zenith angle of 45°.

We have performed simulations to study the dependence of trigger rate on the discriminator threshold keeping the NSB flux level fixed. Discriminator threshold defines photo-electron threshold and hence energy threshold. If we reduce the discriminator threshold the trigger rate will increase. Reducing discriminator threshold results in acceptance of lower energy γ-ray events. However, in reality, using lower discriminator threshold will make the system

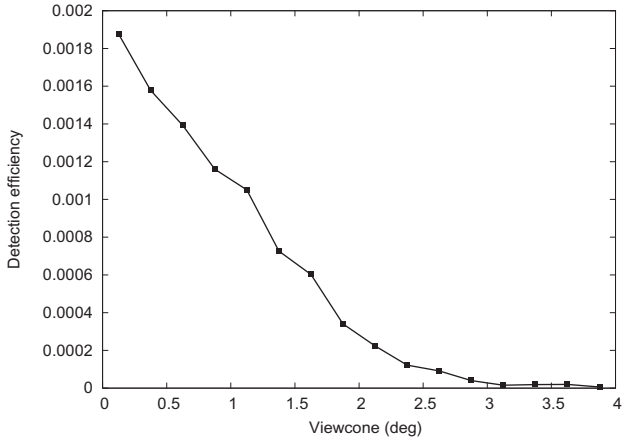

Fig. 9. Detection efficiency vs viewcone for proton showers from simulations for $\geqslant$4-fold trigger condition.

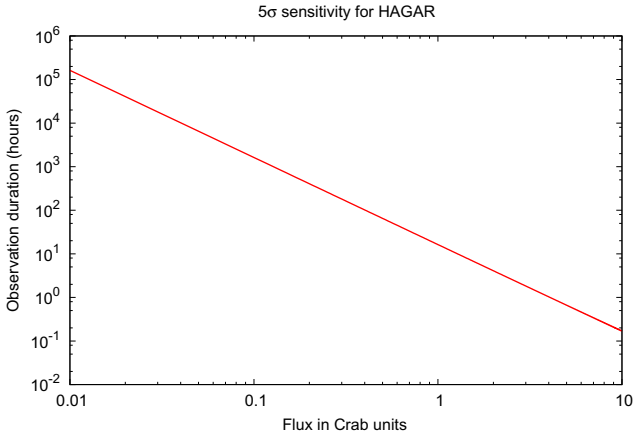

Fig. 10. Observation duration vs source flux for detection of source at 5σ significance level with HAGAR with no additional criteria for the rejection of cosmic ray events.

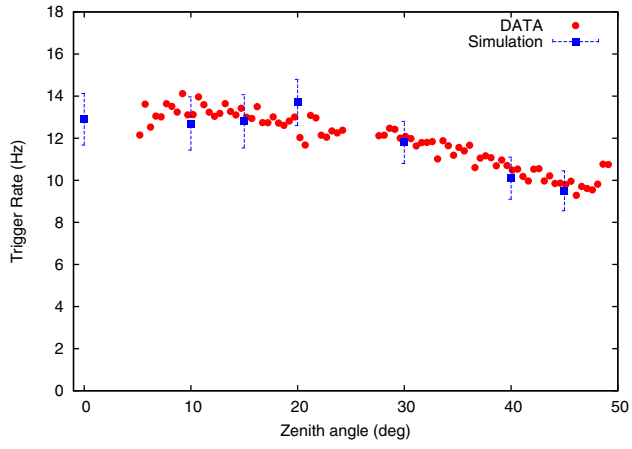

Fig. 11. Trigger rate from MC for different elevation angles.

Table 7
Telescope trigger ratio, R_N, for simulated data, $R_{N,s}$, and for observed data, $R_{N,o}$ with N, the number of telescopes.

N	Simulated trigger ratio $R_{N,s}$	Observed trigger ratio $R_{N,o}$
4	6.4	5.6
5	3.6	3.5
6	1.9	2.0

susceptible to accepting chance events. So we always operate our system at 220 mV (i.e 17.5 single p.h.e) threshold which gives chance rate well within few percent of the trigger rate. Fig. 5 shows the variation of trigger rate with energy threshold (hence photo-electron threshold). These results are given in Table 4 along with thresholds in terms of number of photo-electrons.

Since we encounter different background brightnesses for different sources, the variation of trigger rate with NSB photon flux was also studied. NSB was varied from $(1.0-2.5)\times10^8$ ph cm^{-2} s^{-1} sr^{-1} in steps of 0.5 and PMT gains are changed accordingly to get individual mirror rate of 5 KHz as done in experiment. The royal sum discriminator thresholds are also changed to get royal sum rates within 25–35 KHz. Then the corresponding trigger rates and γ-ray energy thresholds are estimated and are shown in Table 5. Energy threshold decreases as we go from brighter region to darker one.

4.3. Effective area

We have estimated the "effective area" for various trigger conditions. This area is an energy dependent quantity which depends on the details of detector elements and trigger conditions for the detector. The effective area is defined as

$$A_{eff}(E) = \int_0^{r_{max}} \epsilon(r,E)2\pi r dr, \tag{3}$$

where ϵ is the fraction of showers which trigger the system, r_{max} is the maximum impact parameter and E is the energy of the incident primary particle. Fig. 6 shows variation of the effective area with energy for vertically incident γ-ray, proton and alpha particle showers, for trigger condition $\geqslant 4$. Average value of the effective area for $\geqslant 4$ trigger condition is 3.2×10^4 m^2, which decreases for higher fold trigger condition (see Table 2). The effective area also increases with zenith angle (see Table 3).

We have simulated γ-ray showers using γ-ray spectral indices in the range 2.0–3.0. Energy threshold as well as average effective area of the system decreases with the increase of spectral index; see Table 6.

4.4. Detection efficiency

Detection efficiency of γ-rays depends on energy range as well as on the impact parameter range. It increases with the increase of energy of primary particles. For example, for γ-ray energy, E $\geqslant$ 20 GeV, 0.5% of simulated showers trigger the system. But, 5.4% and 25.2% of showers trigger the system for E $\geqslant$ 100 GeV and E $\geqslant$ 1 TeV, respectively. Detection efficiency decreases with the increase of impact parameter. For impact parameter, R $\geqslant$ 0 m, 0.5% of gammas trigger the system and it is only 0.12% for R $\geqslant$ 100 m and 0.01% for R $\geqslant$ 150 m. Proton showers are simulated keeping viewcone, θ, in the range of 0°–4°. Detection efficiency for proton showers also decreases with increase of θ. For $\theta \geqslant 0°$, 0.02% of showers trigger the system. But for $\theta \geqslant 2.5°$, this becomes 0.003%. It should be noted that these numbers are subject to the parameter ranges (energy range, impact parameter range, viewcone range) considered here. Figs. 7–9 show how detection efficiency changes with the change of primary energy, impact parameter and view cone, respectively.

4.5. Sensitivity

Sensitivity of the system is usually expressed as $n\sigma$, where

$$n = \frac{N_{ON}-N_{OFF}}{\sqrt{N_{ON}+N_{OFF}}}, \tag{4}$$

with N_{ON} = number of showers from the source direction which includes γ-ray showers from the source as well as cosmic ray showers

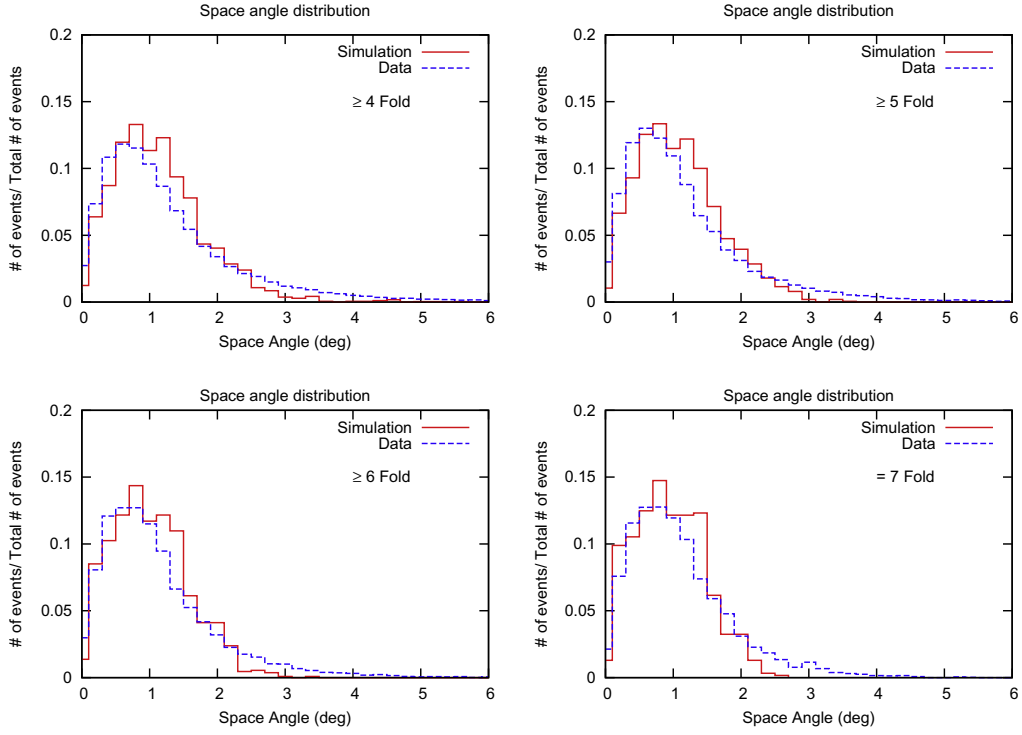

Fig. 12. Comparison of space angle distribution from simulation with observed data, both for vertical directions.

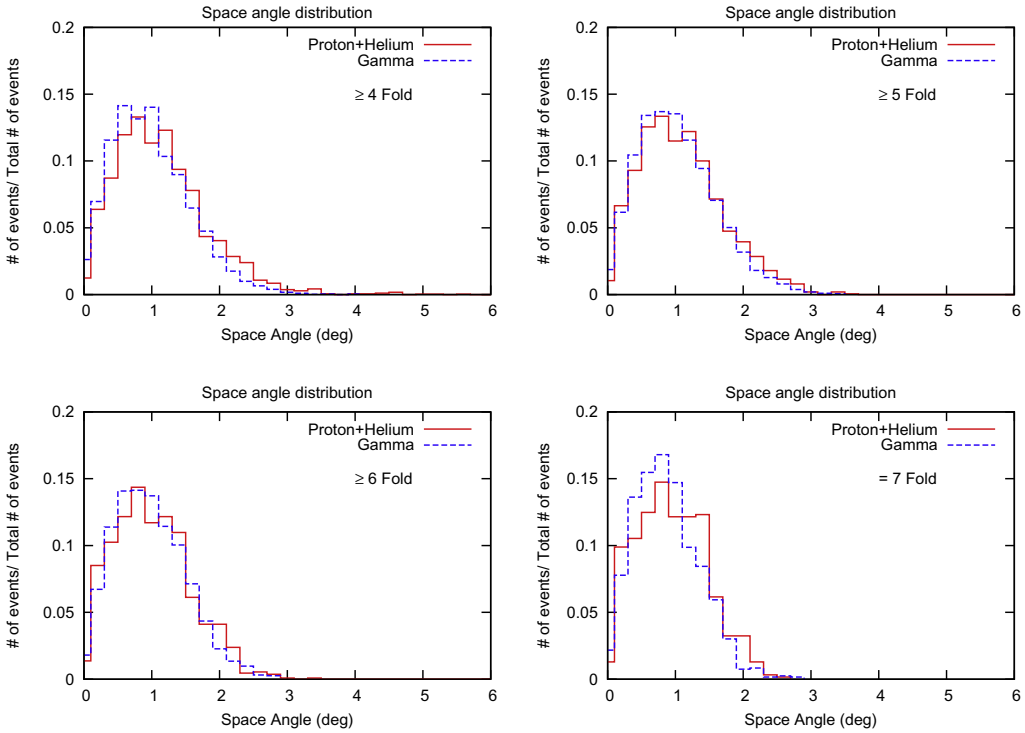

Fig. 13. Comparison of space angle distribution from cosmic ray (proton and helium) showers with γ-ray showers simulations, both for vertical directions.

from the source direction and N_{OFF} = number of background showers (which are essentially cosmic ray showers) away from the source direction.

Eq. (4) can be written as

$$n = R_\gamma\sqrt{t}/\sqrt{R_\gamma + 2(R_p + R_\alpha)}, \tag{5}$$

where R_γ, R_p and R_α are trigger rates of photons, protons and alpha particles respectively and t is the observation duration. We can increase the sensitivity of our measurement by increasing the observation duration of the source. For different sources, R_γ, which is related to the flux from the source, will be different. As a result n also depends on the flux of observed source. So using different flux level we can plot the time duration (t) required to get a given value of the sensitivity, σ. Fig. 10 shows observation duration needed for HAGAR to detect a source at 5σ significance level as a function of source flux in Crab units. This implies that HAGAR will be able to detect Crab nebula like source at a significance level of 5σ in 17 h of observation duration, assuming no additional criteria for the rejection of background cosmic ray events. This corresponds to HAGAR sensitivity for Crab Nebula of $1.2\sigma \times \sqrt{hour}$. This estimate of sensitivity does not include the effect of systematic errors of the instrument. The sensitivity could be improved if more cosmic ray background events are rejected by imposing additional criteria.[2]

5. Comparison of observational data with Monte Carlo simulations

As mentioned earlier, estimate of the cosmic ray trigger rate from our simulations matches well with the observed rate near vertical. For vertical showers the trigger rate obtained from simulations is about 13 Hz which is consistent with the observed trigger rate of about 13.4 Hz. We have also compared variation of trigger rate with zenith angle as obtained from simulations with the data. For this purpose, data obtained by tracking dark region of the sky passing through zenith was used. Fig. 11 shows the comparison of the observed trigger rate as a function of zenith angle with the simulated rates for various zenith angles . A good agreement between the two is seen.

Another check on the performance of the telescope system is provided by the "Telescope Trigger Ratio (TTR)", which we define as follows:

$$R_N \equiv \frac{\text{Number of showers triggering} \geqslant \text{N telescopes}}{\text{Number of showers triggering all 7 telescopes}} \tag{6}$$

Table 7 shows the comparison between simulation and observed data for R_N, indicating a good agreement between the two.

Finally, Fig. 12 shows the comparison of the space angle distributions obtained from simulations and observed data for vertical showers for various trigger conditions. For each triggering event, direction of the shower axis is reconstructed from the TDC data using the plane front approximation for the Cherenkov wavefront. Space angle is defined as the angle between the pointing direction of the telescope system (position of the source in the sky) and reconstructed shower direction. Details about the analysis of data using space angle distribution can be found in [19,20]. There is a fair agreement between the two distributions except for the tail region with larger space angles. We have also compared the space angle distributions between cosmic-ray (proton and helium) showers and γ-ray showers, both obtained from simulations, as shown in Fig. 13. The distributions of space angle for cosmic-ray showers are somewhat broader than the γ-ray showers and it is consistent because of isotropic nature of cosmic-rays.

6. Conclusions

Monte carlo studies show that energy threshold of HAGAR is about 210 GeV. Another setup similar to HAGAR but at lower alti-

[2] Some amount of cosmic rays gets rejected at the trigger level due to the choice of 4-fold or higher fold trigger.

tudes is PACT(Pachmarhi Array of Cherenkov Telescopes)([21–23]) in INDIA. It is installed at Pachmarhi, on the hills of Satpura mountain range, in the state of Madhya Pradesh (Central India). The altitude of PACT is 1075 m amsl. The energy threshold for this PACT array was estimated to be 700–800 GeV, about a factor of 4 higher than that achieved by HAGAR. Thus, by installing the HAGAR system at high altitude it was possible to bring down the energy threshold by a factor of 4 without significantly increasing the mirror area. We have also estimated that this telescope system will be able to detect Crab like sources in 17 h of observations with the significance of 5σ without further rejecting cosmic ray events. Comparison between space angle distributions and variation of trigger rate with zenith angle obtained from simulations are in good agreement with the observed data indicating that HAGAR telescope system is well understood and accurately modeled.

Acknowledgements

We are grateful to the engineering and technical staff of IIA and TIFR who have taken part in the construction of the HAGAR telescopes and contributed to the setting up of the front-end electronics and the data acquisition. We thank Prof. R. Cowsik and Prof. B.V. Sreekantan for their keen interest and encouragement in the development of the HAGAR facility. We would also like to thank the anonymous referees of this paper for their comments and suggestions.

References

[1] W. Galbraith, J.V. Jelley, Nature 171 (1953) 349.
[2] V.R. Chitnis et al., in: Proceedings of 31st ICRC, Łódź, Poland, 2009.
[3] K.S. Gothe et al., Experimental Astronomy, 2012. <http://dx.doi.org/10.1007/s10686-012-9319-9>.
[4] L. Saha et al., in: Proceedings of 32nd ICRC, vol. 9, 2011, p. 198.
[5] R. Britto et al., Astrophys. Space Sci. Trans. 7 (2011) 501.
[6] J. Knapp, D. Heck, Extensive Air Shower Simulation with CORSIKA: A User's Guide, Version 6.7, 2007, p. 7
[7] D. Heck et al., Forschungszentrum Karlsruhe Report FZKA, 1998, p. 6019
[8] K. Werner, Phys. Rep. 232 (1993) 87.
[9] H. Fesefeldt, Report PITHA-85/02, RWTH Aachen, 1985.
[10] W.R. Nelson et al., Report SLAC 265, Stanford Linear Accelerator Center, 1985. <http://www.slac.stanford.edu/pubs/slacreports/slac-r-265.html>, <http://www.irs.inms.nrc.ca/inms/irs/EGS4/getegs4.html>.
[11] K. Bernlohr, Internal report MPI-Heidelberg, 1998, (unpublished) (Astropart. Phys. 12 (2000) 255).
[12] J.R. Horandel, Astropart. Phys. 19 (2003) 193–220.
[13] M. Ackermann et al., PRD 82 (2010) 092004.
[14] A.M. Hillas et al., Astrophys. J. 503 (1998) 744.
[15] F.A. Aharonian et al., Astrophys. J. 539 (2000) 317.
[16] F.A. Aharonian et al., Astron. & Astrophys. 457 (2006).
[17] D. Bose, PhD Thesis, Tata Institute of Fundamental Research, Unpublished, 2007.
[18] C.W. Allen, Astrophys. Quantities, 1955.
[19] R.J. Britto et al., ICRC, OG 2.5, abstract ID 943, 2011.
[20] A. Shukla et al., Astron. & Astrophys. 541 (2012) A140.
[21] P. Majumdar et al., Astropart. Phys. 18 (2003) 333.
[22] D. Bose et al., Astrophys. Space Sci. 309 (2007) 111.
[23] B.B. Singh et al., Astropart. Phys. 32 (2009) 120.